RSC Advances

PAPER

View Article Online
View Journal | View Issue

Cite this: *RSC Adv.*, 2025, **15**, 19696

Synthesis of Mo, N-doped carbon dots for the fluorescence detection of $Cr_2O_7^{2-}$ and luteolin and their application in anti-counterfeiting†

Yang Geng, *[ab] Ze-Yue Zhao,[a] Wei Zhang,[a] Bai-Qiang Zhai,[a] Ye Tian*[a] and Wen-Zhu Bi *[c]

In this work, Mo, N-doped carbon dots (Mo, N-CDs) were synthesized *via* a one-step hydrothermal method using L-arginine, ammonium molybdate and 1-pyrenecarboxaldehyde as precursors. The synthetic conditions, morphological structure, elemental composition and optical properties of Mo, N-CDs were carefully optimized and characterized. The as-synthesized Mo, N-CDs displayed cyan fluorescence emission at 494 nm with a high quantum yield (41.5%) and demonstrated superior pH stability, salt tolerance, thermostability and photobleaching resistance. In addition, Mo, N-CDs were employed as "on–off" sensors for the detection of $Cr_2O_7^{2-}$ and luteolin with excellent linear correlation over a wide linear range (0–50 μM and 0–45 μM, respectively), low detection limits (0.96 μM and 0.64 μM, respectively) and short response time (<10 s). In addition, the practical detection of $Cr_2O_7^{2-}$ and luteolin in actual samples demonstrated good recoveries (93–110%) with relative standard deviations less than 5%. Furthermore, the Mo, N-CD aqueous solution was directly used as a fluorescent ink and exhibited excellent anti-counterfeiting effects.

Received 14th March 2025
Accepted 18th May 2025

DOI: 10.1039/d5ra01824b

rsc.li/rsc-advances

Introduction

Dichromate ion ($Cr_2O_7^{2-}$) is a dangerous oxygen-containing anion and is hazardous to the environment and organisms.[1] With its wide use in chemical industries (electroplating, metallurgy, paint and leather tanning), $Cr_2O_7^{2-}$ has become the most common heavy metal pollutant in water.[2] Therefore, accurate detection of $Cr_2O_7^{2-}$ in water is essential for environmental water monitoring and safeguarding biological health. Traditional methods for the detection of $Cr_2O_7^{2-}$, such as atomic absorption spectrometry,[3] inductively coupled plasma mass spectrometry (ICP-MS),[4] and colorimetric and electrochemical analyses,[5] usually require expensive instruments and tedious operation procedures, which limit their application in the fast detection of $Cr_2O_7^{2-}$. Luteolin (3,4,5,7-tetrahydroxyflavone) is a natural flavonoid compound with various pharmacological effects, such as antimicrobial, anti-inflammatory and antioxidant effects.[6] Therefore, the detection of luteolin is of great practical importance in pharmaceutical analyses. Common methods for the detection of luteolin, including electrochemical methods,[7] capillary zone electrophoresis (CZE),[8] high-performance liquid chromatography (HPLC)[9] and spectrophotometry (SP),[10] have the drawbacks of high cost, low sensitivity and being time-consuming. Therefore, there is an urgent need for the development of new methods for fast and real-time detection of $Cr_2O_7^{2-}$ and luteolin.

In order to address this issue, fluorescent detection strategies, especially carbon dot (CD)-based fluorescence strategies, stand out owing to their low-cost fabrication, low cytotoxicity, simple operation procedure, high sensitivity and selectivity and rapid response time.[11,12] In the past years, numerous CD-based fluorescence sensors have been reported for the detection of $Cr_2O_7^{2-}$ (for more details see Table S1†)[13] and luteolin.[14] However, these sensors often have the defects of low fluorescence quantum yield (FLQY), long response time and insufficient stability, which greatly limit their fluorescence detection applications. To solve these problems, researchers have found that doping CDs with heteroatoms can significantly improve their FLQY.[15] Among them, non-metallic atom (N, B, P and S)[16–19]-doped CDs are frequently reported, while metal atom-doped CDs are relatively less reported and mainly focus on limited metal ions (Co, Cu, Fe and Zn).[20,21] As an important transition metal element with high biocompatibility and good stability, molybdenum (Mo) has been reported for the synthesis of numerous functionalized molybdenum disulfide (MoS_2) nanomaterials with different sulfur sources.[22,23] However, Mo-doped CDs are rarely reported in literature.[24]

[a]*Department of Pharmacy, Zhengzhou Railway Vocational and Technical College, Zhengzhou, 451460, China. E-mail: tianye@zzrvtc.edu.cn*

[b]*Henan Railway Food Safety Management Engineering Technology Research Center, Zhengzhou Railway Vocational and Technical College, Zhengzhou, 451460, China*

[c]*School of Pharmacy, Henan University of Chinese Medicine, Zhengzhou, 450046, China. E-mail: biwenzhu2018@hactcm.edu.cn*

† Electronic supplementary information (ESI) available. See DOI: https://doi.org/10.1039/d5ra01824b

Scheme 1 Synthesis of Mo, N-CDs for $Cr_2O_7^{2-}$ and luteolin detection.

To enrich the scope of heteroatom-doped CDs and construct a fast detection platform for $Cr_2O_7^{2-}$ and luteolin, we report a facile synthesis of Mo, N-doped CDs (Mo, N-CDs) using L-arginine,[25] ammonium molybdate and 1-pyrenecarboxaldehyde as precursors *via* a simple one-step hydrothermal route (Scheme 1). The as-prepared Mo, N-CDs exhibited cyan fluorescence under a 365 nm UV light with a high FLQY of 41.5%. The morphology, structure and elemental composition of Mo, N-CDs were carefully characterized, indicating that molybdenum and nitrogen atoms were successfully doped. Further investigations showed that Mo, N-CDs exhibit good pH stability, salt tolerance, thermostability and photobleaching resistance. Moreover, Mo, N-CDs could be employed as "on–off" sensors for the sensitive detection of $Cr_2O_7^{2-}$ and luteolin with low detection limits (0.96 and 0.64 μM) and wide linear range (0–50 μM, $R^2 = 0.9956$ and 0–45 μM, $R^2 = 0.9992$). Furthermore, the detection of $Cr_2O_7^{2-}$ and luteolin in actual water samples and drugs was also investigated and showed acceptable recoveries (93–110%) with relative standard deviations of less than 5%. In addition, the application of Mo, N-CDs as fluorescent ink was explored and demonstrated excellent anti-counterfeiting effects.

Results and discussion

Synthesis and characterization

Initially, the hydrothermal reaction conditions and the molybdenum source for the preparation of Mo, N-CDs were optimized. As shown in Table S2,† 1-pyrenecarboxaldehyde and ammonium molybdate were indispensable (entries 1–4) and the highest fluorescence intensity of Mo, N-CDs was obtained with L-arginine (0.3 g), ammonium molybdate (0.3 g) and 1-pyrenecarboxaldehyde (0.02 g) under the optimal hydrothermal conditions (190 °C, 4 h as shown in entry 2 in Table S2†).

Then, the morphology structure of Mo, N-CDs was characterized by transmission electron microscopy (TEM), X-ray diffraction (XRD) and Raman spectroscopy (Fig. 1 and S2†). The TEM image showed that Mo, N-CDs were nearly spherical with a particle diameter of 1.7 ± 0.04 nm (Fig. 1a and b). High-resolution TEM (HRTEM) images showed Mo, N-CDs with a carbon core structure and lattice fringes of approximately 0.15 nm (Fig. 1c). Typical XRD pattern of Mo, N-CDs showed a broad peak at about 24.2°, corresponding to the peak of graphite (002) (Fig. 1d).[26] Raman spectrum of Mo, N-CDs showed the main peak at around 1400 cm^{-1} (D band) and the shoulder peak at around 1600 cm^{-1} (G band), respectively, which should be assigned to disordered structures of the sp^2 domains and in-plane vibrations of crystalline graphite

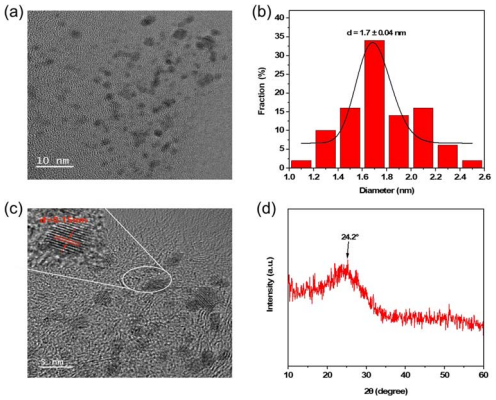

Fig. 1 (a) TEM image; (b) particle size distribution histogram and curve; (c) HRTEM image; and (d) XRD pattern of Mo, N-CDs.

(Fig. S2†).[25d] These results were compatible with the features of carbon dots.[27]

The surface functional groups of Mo, N-CDs were analyzed by Fourier transform infrared spectroscopy (FTIR). As shown in Fig. 2a, the broad absorption peaks at 3130 and 3010 cm^{-1} indicating the existence of N–H/O–H bonds.[28] The peaks at 2916, 2848 and 1490 cm^{-1} indicated the C–H bonds.[29] The two peaks at 1584 and 1400 cm^{-1} showed conjugated C=N, C=O and C=C bonds.[30] The two peaks at 1435 and 1166 cm^{-1} indicated the existence of C–N and C–O bonds.[31] The peak at 893 cm^{-1} should be the evidence of the existence of Mo–O bond.[32] The elemental compositions of Mo, N-CDs were characterized by X-ray photoelectron spectroscopy (XPS). The full-scan XPS spectrum (Fig. 2b) shows distinct peaks at 232.23, 284.91, 399.55 and 530.56 eV, representing the presence of Mo3d (4.94%), C 1s (41.08%), N 1s (29.18%) and O 1s (24.79%),

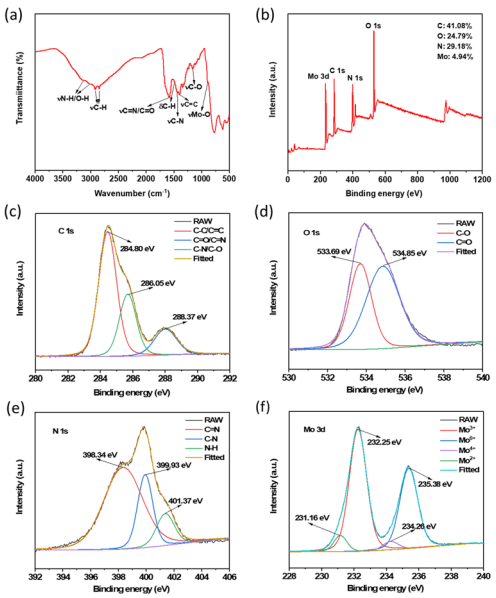

Fig. 2 (a) FTIR spectrum of Mo, N-CDs and (b–f) XPS spectra of Mo, N-CDs: (b) full scan; (c–f) high-resolution spectrum of C 1s, O 1s, N 1s and Mo 3d.

respectively. The high-resolution C 1s spectrum (Fig. 2c) showed three fitted peaks at 284.80, 286.05 and 288.37 eV, corresponding to C–C/C=C, C–N/C–O and C=O/C=N bonds.[31,33] The high-resolution O 1s spectrum (Fig. 2d) showed two fitted peaks at 533.69 and 534.85 eV, corresponding to the C–O and C=O bonds.[34] Three fitted peaks at 398.34, 399.93 and 401.37 eV in the high-resolution N 1 s spectrum (Fig. 2e) inferred the C=N, C–N and N–H bonds.[35] Four fitted peaks at 231.16, 232.25, 234.26 and 235.38 eV in the high-resolution Mo 3d spectrum (Fig. 2f) corresponded to Mo^{2+}, Mo^{3+}, Mo^{4+} and Mo^{6+}.[36] Furthermore, the presence of C, O, N and Mo in Mo,N-CDs was explored using the EDX spectrum (Fig. S3†).[25d] These results indicated that molybdenum and nitrogen were successfully doped in the as-synthesized carbon dots in this work.

Optical properties

The optical properties of Mo, N-CDs were investigated by UV-vis absorption and fluorescence spectroscopy. Mo, N-CDs showed strong absorption at 274 nm and weak absorption at 326 and 342 nm, which corresponded to the π–π* transition of C=C bonds and n–π* transition of C=N/C=O bonds.[37,38] Fluorescence spectra showed that the maximum excitation/emission wavelengths of Mo, N-CDs were 365/494 nm (Fig. 3a). Therefore, the Mo, N-CD aqueous solution appeared colourless under sunlight and cyan under UV irradiation (365 nm, insets of Fig. 3a). When the excitation wavelength was varied from 355 to 435 nm, the emission peaks of Mo, N-CDs remained almost unchanged, showing an excitation-wavelength-independent emission property (Fig. 3b). The fluorescence quantum yield (FLQY) of Mo, N-CDs was calculated to be 41.5% using quinine sulphate as a reference (Fig. S4†).

The stability of Mo, N-CDs was also investigated to evaluate their feasibility in natural environments (Fig. 3c–f). The fluorescence intensities of Mo, N-CDs did not show significant changes under continuous excitation irradiation at 365 nm for 90 min, different pH (3–12), NaCl concentrations (0–100 mM) and incubation temperatures (5–85 °C), demonstrating the excellent photobleaching resistance, pH stability, salt tolerance and thermostability of Mo, N-CDs.

Detection of $Cr_2O_7^{2-}$

The recognition ability of Mo, N-CDs was studied by adding 25 common ions to the Mo, N-CD aqueous solution (Ag^+, Al^{3+}, Ba^{2+}, Ca^{2+}, Cd^{2+}, Cr^{3+}, Cu^{2+}, Hg^{2+}, K^+, Mg^{2+}, Na^+, NH_4^+, Ni^{2+}, Sn^{2+}, Zn^{2+}, Br^-, Cl^-, ClO_4^-, CO_3^{2-}, $Cr_2O_7^{2-}$, F^-, I^-, NO_3^-, PO_4^{3-} and SO_4^{2-}). As shown in Fig. 4a, $Cr_2O_7^{2-}$ quenched the fluorescence of Mo, N-CDs, whereas the other ions can hardly change the fluorescence of Mo, N-CDs. The anti-interference ability of Mo, N-CDs was studied through the addition of $Cr_2O_7^{2-}$ to Mo, N-CD solutions containing other ions (Fig. 4b). The results showed that the selectivity of Mo, N-CDs for $Cr_2O_7^{2-}$ was not affected. Response time studies showed that $Cr_2O_7^{2-}$ could instantly (<10 s) quench the fluorescence of Mo, N-CDs (Fig. S5†). The sensitivity was explored by the measurements of fluorescence intensities of Mo, N-CDs with different amounts of $Cr_2O_7^{2-}$. As shown in Fig. 4c, the fluorescence intensity decreased with the gradual increase of $Cr_2O_7^{2-}$. The quenching efficiency was determined by F/F_0, where F_0 is the intensity of the blank Mo, N-CD solution and F is the intensity of the Mo,N-CDs with $Cr_2O_7^{2-}$. A linear curve was obtained by plotting the quenching efficiency *vs.* $Cr_2O_7^{2-}$ (0–50 μM). As shown in Fig. 4d, the linear equation was calculated to be $F/F_0 = -0.0086\ C(Cr_2O_7^{2-}) + 0.9904$ with a correlation coefficient (R^2) of 0.9956. The detection limit (LoD) was 0.96 μM (calculated using the ($3\sigma/k$)

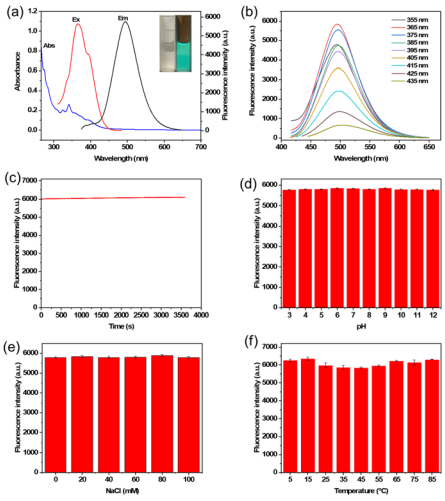

Fig. 3 (a) UV-vis absorption and fluorescence spectra of Mo, N-CDs (insets: images of Mo, N-CDs under sunlight (left) and under a 365 nm UV light (right)); (b) fluorescence emission spectra of Mo, N-CDs under different excitation conditions; (c) fluorescence intensities of Mo, N-CDs at 494 nm at a continuous excitation of 365 nm; and (d–f) fluorescence intensity of Mo, N-CDs at different pH, NaCl concentration and incubation temperatures, respectively.

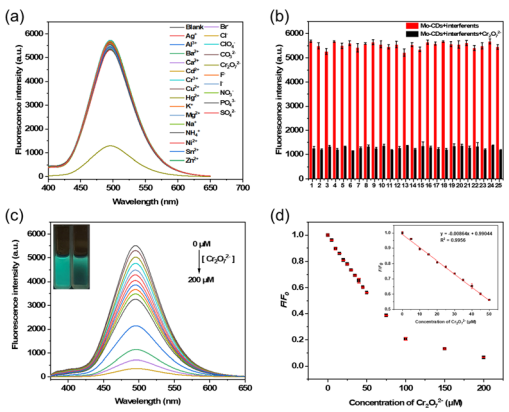

Fig. 4 (a) Fluorescence spectra of Mo, N-CDs with different ions (100 μM); (b) fluorescence intensities of Mo, N-CDs with different ions (1–25: blank, Ag^+, Al^{3+}, Ba^{2+}, Ca^{2+}, Cd^{2+}, Cr^{3+}, Cu^{2+}, Hg^{2+}, K^+, Mg^{2+}, Na^+, NH_4^+, Ni^{2+}, Sn^{2+}, Zn^{2+}, Br^-, Cl^-, ClO_4^-, CO_3^{2-}, F^-, I^-, NO_3^-, PO_4^{3-} and SO_4^{2-}) in the absence (red)/presence (black) of $Cr_2O_7^{2-}$ (100 μM); (c) fluorescence emission spectra of Mo, N-CDs with different concentrations of $Cr_2O_7^{2-}$ (inset: photograph of the Mo, N-CD solution without (left)/with (right) $Cr_2O_7^{2-}$ (100 μM) under a 365 nm UV light); and (d) relationship between F/F_0 and the concentration of $Cr_2O_7^{2-}$.

method, where σ is the standard deviation of the blank sample ($n = 10$) (Table S3†) and k is the slope of the linear calibration curve). Compared to previously published works for the detection of $Cr_2O_7^{2-}$ (as listed in Table S1†), Mo, N-CDs in this work showed a fast response to $Cr_2O_7^{2-}$ with a wide linear range and acceptable detection limit (<50 μg L^{-1} by WHO).[37,39] In summary, Mo, N-CDs are promising for the rapid quantitative analysis of $Cr_2O_7^{2-}$ in aqueous solution.

Detection of luteolin

In this experiment, 10 compounds (glutathione (GSH), glucose, L-arginine (L-Arg), L-cysteine (L-Cys), L-glutamic acid (L-Glu), luteolin, nicotinamide, ascorbic acid (AA), citric acid (CA) and urea) were selected to explore the selectivity and anti-interference capability of Mo, N-CDs. As shown in Fig. 5a–b, the fluorescence of Mo, N-CDs was significantly quenched by luteolin, whereas the other compounds did not influence the detection of luteolin. The exploration of response time showed that the fluorescence intensity of Mo, N-CDs was also instantly (<10 s) quenched by luteolin (Fig. S6†). The sensitivity of Mo,N-CDs to luteolin was explored using the same method for $Cr_2O_7^{2-}$. As shown in Fig. 5c and d, the quenching efficiency F/F_0 *vs.* luteolin (0–45 μM) was plotted, and the linear equation was $F/F_0 = -0.0129\ C$ (luteolin) + 0.9920 with a correlation coefficient (R^2) of 0.9992. The detection limit is 0.64 μM, calculated using the ($3\sigma/k$) method. Compared with previous works,[14] Mo, N-CDs in this work showed a fast response to luteolin with a low detection limit. These results show that Mo, N-CDs can be used for quantitative detection of luteolin *in vitro*.

Quenching mechanism for $Cr_2O_7^{2-}$

The mechanism of fluorescence quenching was explored through UV-vis and fluorescence spectroscopy, zeta potential and fluorescence lifetime measurements. As shown in Fig. 6,

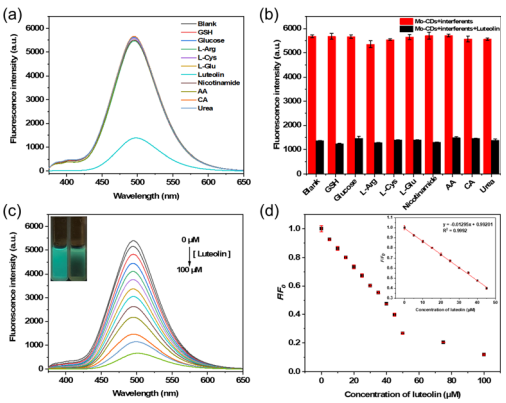

Fig. 5 (a) Fluorescence spectra of Mo, N-CDs with different compounds (luteolin (50 μM), other compounds (100 μM)); (b) fluorescence intensities of Mo, N-CDs with different compounds in the absence (red)/presence (black) of luteolin (50 μM); (c) fluorescence spectra of Mo, N-CDs with different concentrations of luteolin (inset: photographs of the Mo, N-CD solution without (left)/with (right) luteolin (50 μM) under a 365 nm UV light); and (d) relationship between F/F_0 and the concentration of luteolin.

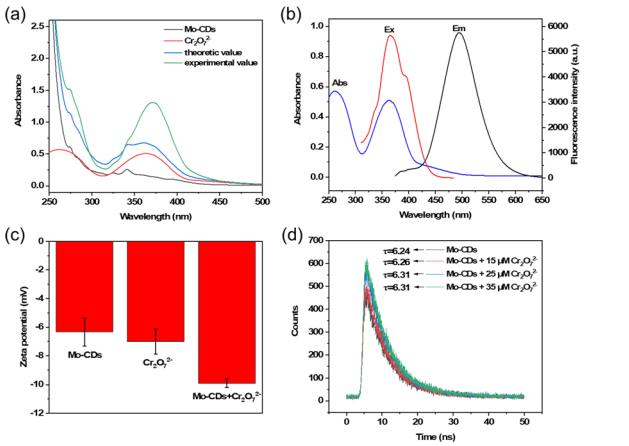

Fig. 6 (a) UV-vis spectra of Mo, N-CDs, $Cr_2O_7^{2-}$, theoretical and experimental spectra of Mo, N-CDs/$Cr_2O_7^{2-}$; (b) UV-vis spectrum of $Cr_2O_7^{2-}$ and fluorescence spectra of Mo, N-CDs; (c) zeta potentials of Mo, N-CDs, $Cr_2O_7^{2-}$ and Mo, N-CDs/$Cr_2O_7^{2-}$; and (d) fluorescence lifetime of Mo, N-CDs (without/with $Cr_2O_7^{2-}$).

compared to the theoretical UV-vis absorption spectra, the Mo, N-CDs/$Cr_2O_7^{2-}$ mixtures did not give new absorption peaks, which ruled out the formation of non-fluorescent ground state complexes (Fig. 6a).[40] Additionally, as illustrated in Fig. 6b, the UV-vis spectrum of $Cr_2O_7^{2-}$ overlapped with the fluorescence spectra of Mo, N-CDs, indicating that the quenching mechanism might be inner-filter effect (IFE) and fluorescence resonance energy transfer (FRET).[41] The negative zeta potential (−6.34 and −9.90 mV) indicated no electrostatic attraction between Mo, N-CDs and $Cr_2O_7^{2-}$ (Fig. 6c), and unchanged fluorescence lifetime (6.24, 6.26, 6.31 and 6.31 ns) ruled out the FRET quenching mechanism (Fig. 6d).[42] Therefore, an IFE mechanism was proposed for sensing $Cr_2O_7^{2-}$.

To calculate the IFE ratio, a series of Mo, N-CD solutions with different amounts of $Cr_2O_7^{2-}$ were prepared, and their absorbance values (A_{ex} and A_{em}) and fluorescence intensities (F_{obsd}) were measured. Then, the corrected fluorescence emission intensities (F_{cor}) were calculated according to Parker's equation (eqn (1)).[43] Thereafter, the correction factor (CF), observed fluorescence suppression efficiency (E_{obsd}) and corrected fluorescence suppression efficiency (E_{cor}) were calculated, as shown in Table 1 (CF < 3 to ensure the accuracy of the results). The IFE ratio was calculated as ($E_{obsd} - E_{cor}$)/E_{obsd} to be 95.34%.[44] The ratio of the corrected fluorescence emission intensities without/with $Cr_2O_7^{2-}$ ($F_{cor.o}/F_{cor}$) *versus* the concentration of $Cr_2O_7^{2-}$ were plotted as shown in Fig. S8.† $F_{cor,0}/F_{cor}$ was not linearly related with $Cr_2O_7^{2-}$, which further ruled out the static and dynamic quenching effects in this system according to the Stern–Volmer equation eqn (2).[44]

$$\frac{F_{cor}}{F_{obsd}} = \frac{2.3dA_{ex}}{1-10^{-dA_{ex}}}10^{gA_{em}}\frac{2.3sA_{em}}{1-10^{-sA_{em}}} \quad (1)$$

F_{cor} and F_{obsd} are the corrected and measured fluorescence intensities at 494 nm; d, g and s are the geometric parameters of the quartz cuvette (shown in Fig. S7,† 1.00, 0.25 and 0.50 cm, respectively); and A_{ex} and A_{em} are the absorbance at the

Table 1 Calculation of the IFE ratio for $Cr_2O_7^{2-}$[a]

$Cr_2O_7^{2-}$ (μM)	A_{ex}	A_{em}	F_{obsd}	F_{cor}	CF	E_{obsd}	E_{cor}
0	0.52	0.025	5212	9198	1.76	0.00	0.000
5	0.56	0.020	5050	9158	1.82	0.03	0.001
10	0.62	0.024	4658	8991	1.93	0.11	0.022
15	0.66	0.019	4432	8804	1.99	0.15	0.043
20	0.72	0.016	4161	8651	2.08	0.20	0.059
25	0.80	0.042	3950	9075	2.30	0.24	0.013

[a] $CF = F_{cor}/F_{obsd}$; $E_{obsd} = 1 - F_{obsd}/F_{obsd.0}$; $E_{cor} = 1 - F_{cor}/F_{cor.0}$ ($F_{obsd.0}$ and $F_{cor.0}$ are the measured and corrected fluorescence intensities, respectively, without $Cr_2O_7^{2-}$).

Table 2 Calculation of the IFE ratio for luteolin[a]

Luteolin (μM)	A_{ex}	A_{em}	F_{obsd}	F_{cor}	CF	E_{obsd}	E_{cor}
0	0.63	0.039	5786	11475	1.98	0.00	0.000
5	0.68	0.049	5390	11310	2.10	0.07	0.014
10	0.78	0.049	4865	11095	2.28	0.16	0.033
15	0.94	0.067	4119	10831	2.63	0.29	0.056
20	1.02	0.069	3809	10712	2.81	0.34	0.066
25	0.63	0.039	5786	11475	1.98	0.00	0.000

[a] $CF = F_{cor}/F_{obsd}$; $E_{obsd} = 1 - F_{obsd}/F_{obsd.0}$; $E_{cor} = 1 - F_{cor}/F_{cor.0}$ ($F_{obsd.0}$ and $F_{cor.0}$ are the measured and corrected fluorescence intensities, respectively, without luteolin).

excitation wavelength (365 nm) and the optimal emission wavelength (494 nm).

$$F_{cor.0}/F_{cor} = 1 + K_{SV}[Q] \quad (2)$$

$F_{cor.0}$ and F_{cor} are the corrected fluorescence intensities without and with $Cr_2O_7^{2-}$; K_{sv} is the Stern–Volmer constant; $[Q]$ is the concentration of $Cr_2O_7^{2-}$.

Quenching mechanism of luteolin

The possible mechanism of luteolin detection was investigated using the same method described above. As shown in Fig. 7a, a new absorption band was formed at 379–390 nm in the experimental UV-vis absorption spectrum of the Mo, N-CDs/luteolin mixture, indicating the formation of non-fluorescent ground state complexes and a static quenching mechanism.[45] Fig. 7b indicates that the quenching mechanism of Mo, N-CDs for luteolin might be IFE and FRET.[46] Zeta potential measurements showed that no electrostatic interaction existed between Mo, N-CDs and luteolin (Fig. 7c), and fluorescence lifetime measurements ruled out FRET (Fig. 7d). In addition, the IFE ratio was calculated to be 80.55% (Table 2)[43] and the presence of a static quenching effect was verified by the Stern–Volmer equation (Fig. S9†).[47] In summary, the combination of IFE and static quenching may be the mechanism by which Mo, N-CDs detect luteolin.

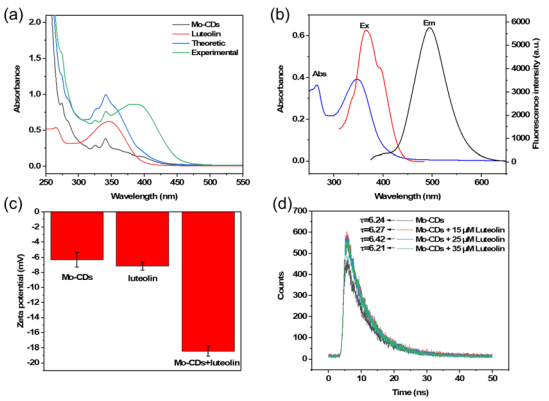

Fig. 7 (a) UV-vis spectra of Mo, N-CDs, luteolin, theoretical and experimental spectra of Mo, N-CDs/luteolin; (b) UV-vis spectrum of luteolin and fluorescence spectra of Mo, N-CDs; (c) zeta potentials of Mo, N-CDs, luteolin and Mo, N-CDs/luteolin; and (d) fluorescence lifetime of Mo, N-CDs (without/with luteolin).

Testing of actual samples

The detection of $Cr_2O_7^{2-}$ and luteolin in actual samples was further investigated to validate the reliability of the method. As shown in Tables 3 and 4, the recoveries of $Cr_2O_7^{2-}$ in tap water, lake water and bottled drinking water and luteolin in Du Yi Wei capsule and Du Yi Wei tablet were 93–110% with relative standard deviations (RSD) less than 5%. Therefore, Mo, N-CDs can be used as "on-off" sensors for the detection of $Cr_2O_7^{2-}$ and luteolin in the field of water quality monitoring and pharmaceutical analysis.

Anti-counterfeiting application

Due to their stable optical property and relatively high quantum yields, Mo, N-CDs have potential application prospects in anti-counterfeiting. As shown in Fig. 8, two pictures were drawn by hand on test paper using a Mo, N-CD aqueous solution as fluorescent ink. The two pictures were almost invisible under sunlight but exhibited obvious cyan fluorescence under 365 nm UV light, showing good fluorescence anti-counterfeiting effects. With the removal of 365 nm UV light, the cyan fluorescence disappeared completely, demonstrating high-quality information encryption and decryption effects. The maintenance of fluorescence for several months indicates that the Mo, N-CD-based fluorescent ink exhibits better durability and reliability.

Table 3 Detection of $Cr_2O_7^{2-}$ in actual water samples ($n = 3$)

Samples	Spiked (μM)	Found (μM)	Recovery (%)	RSD (%)
Tap water	15	14.67	97.78	0.46
	25	25.17	100.68	0.23
	35	34.51	98.61	1.27
Lake water	15	16.44	109.64	0.86
	25	24.29	97.15	0.15
	35	35.74	102.12	2.05
Bottled drinking water	15	14.51	96.73	0.76
	25	25.52	102.10	0.22
	35	36.19	103.41	0.28

Table 4 Detection of luteolin in actual samples ($n = 3$)

Samples	Spiked (μM)	Found (μM)	Recovery (%)	RSD (%)
Du Yi Wei capsule	0	5.26	—	0.83
	15	20.91	104.26	1.97
	25	29.94	98.71	1.24
	35	37.88	93.18	2.23
Du Yi Wei tablet	0	3.10	—	3.39
	15	18.53	102.85	0.25
	25	28.48	101.50	1.08
	35	36.67	95.92	2.71

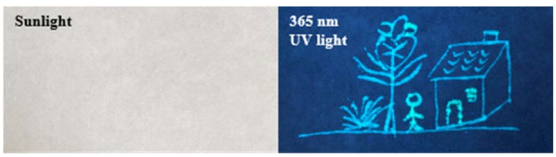

Fig. 8 Photographs of pictures drawn by hand using Mo, N-CDs as fluorescent ink on test paper under sunlight (left) and under a 365 nm UV light (right).

Conclusions

In conclusion, a rarely reported Mo, N-doped cyan fluorescent carbon dots (Mo, N-CDs) was successfully synthesized by a one-step hydrothermal method using L-arginine, ammonium molybdate and indispensable 1-pyrenecarboxaldehyde as precursors. The results of morphological and compositional characterization showed that molybdenum and nitrogen atoms were successfully doped into carbon dots. Due to its high quantum yield, superior pH stability, salt tolerance and excellent photobleaching resistance, a fluorescence platform based on Mo, N-CDs was constructed for "on–off" detection of $Cr_2O_7^{2-}$ and luteolin in aqueous solutions and actual samples. This method demonstrated high selectivity and sensitivity, a short response time and satisfactory recoveries. The fluorescence quenching mechanisms of Mo, N-CDs were explored and putatively identified as IFE (95.34%) for $Cr_2O_7^{2-}$ and IFE (80.55%)/static quenching for luteolin. Furthermore, an aqueous solution of Mo, N-CDs can be directly used as a fluorescent ink and exhibits excellent anti-counterfeiting effects. The facial synthesis, high quantum yield, stable optical properties and rapid responsiveness of Mo, N-CDs make them an excellent alternative in environmental water monitoring and pharmaceutical analysis as well as anti-counterfeiting.

Data availability

The data supporting this article have been included as part of the ESI.†

Author contributions

Yang Geng and Ze-Yue Zhao: methodology, formal analysis, investigation, and writing – review and editing. Wei Zhang and Bai-Qiang Zhai: conceptualization and analysis. Ye Tian and Wen-Zhu Bi: validation and supervision.

Conflicts of interest

There are no conflicts to declare.

Acknowledgements

This work was supported by Henan Provincial Science and Technology International Cooperation Grant (242102521040), the Science and Technology Development Plan Project Henan Province (242102311178) and the Key Research Project of Zhengzhou Railway Vocational and Technical College (2025KY005).

Notes and references

1 (*a*) Z. Yu, C. Deng, S. Jiang, Y. Liu, C. Liu, F. Seidi, X. Zhang, Y. Huang, W. Wu, J. Han, Q. Yong and H. Xiao, *J. Colloid Interface Sci.*, 2025, **679**, 510; (*b*) T. Zheng, L. Qian, M. Li, Z. Wang, K. Li, Y. Zhang, B. Li and B. Wu, *Dalton Trans.*, 2018, **47**, 9103; (*c*) B. Prathima, V. S. Raghvan, S. Soni, S. S. Gorthi and G. L. Sivakumar Babu, *J. Water Process. Eng.*, 2024, **66**, 105832.

2 D. M. Hausladen, A. A. Ozinskas, C. N. McClain and S. Fendorf, *Environ. Sci. Technol.*, 2018, **52**, 8242.

3 (*a*) F. A. S. Cunha, J. P. A. Fernandes, W. S. Lyra, A. G. G. Pessoa, J. C. C. Santos, M. C. U. Araújo and L. F. Almeida, *J. Anal. At. Spectrom.*, 2024, **39**, 1398; (*b*) Z. Tahmasebi, S. S. H. Davarani, H. Ebrahimzadeh and A. A. Asgharinezhad, *Microchem. J.*, 2018, **143**, 212.

4 R. Pechancová, T. Pluháček, J. Gallo and D. Milde, *Talanta*, 2018, **185**, 370.

5 (*a*) S. Liu, X. Wang, C. Zou, J. Zhou, M. Yang, S. Zhang, D. Huo and C. Hou, *Anal. Chim. Acta*, 2021, **1149**, 238141; (*b*) F. Yao, M. Jia, Q. Yang, K. Luo, F. Chen, Y. Zhong, L. He, Z. Pi, K. Hou, D. Wang and X. Li, *Chemosphere*, 2020, **260**, 127537; (*c*) J. Wan, M. Yu, W. Bi, Y. Sun, W. Wang, Y. Hou, S. Xie, T. Li and Y. Fan, *J. Water Process. Eng.*, 2024, **68**, 106447; (*d*) I. Kabdaşli and O. Tünay, *Molecules*, 2023, **28**, 2411.

6 (*a*) A. S. U. Mahamud, M. Ashrafudoulla, S. Nahar, M. A. H. Chowdhury, S. H. Park and S. D. Ha, *Food Control*, 2024, **166**, 110734; (*b*) S. F. Nabavi, N. Braidy, O. Gortzi, E. S. Sanchez, M. Daglia, K. S. Woźniak and S. M. Nabavi, *Brain Res. Bull.*, 2015, **119**, 1; (*c*) N. Aziz, M. Y. Kim and J. Y. Cho, *J. Ethnopharmacol.*, 2018, **225**, 342; (*d*) M. Zhu, Y. Sun, Y. Su, W. Guan, Y. Wang, J. Han, S. Wang, B. Yang, Q. Wang and H. Kuang, *Phytother. Res.*, 2024, **38**, 3417.

7 (*a*) B. Wang, W. Zhao, L. Wang, K. Kang, X. Li, D. Zhang, J. Ren and X. Ji, *Talanta*, 2024, **273**, 125836; (*b*) X. Hou, W. Wu, F. Zhao, W. Xie and Q. Yang, *Microchim. Acta*, 2021, **188**, 86; (*c*) X. Li, R. Zou, Y. Niu, W. Sun, T. Shao and X. Chen, *Sensors*, 2018, **18**, 2309.

8 Y. Li, Q. Zhang, H. Sun, N. K. Cheung and H. Y. Cheung, *Talanta*, 2013, **105**, 393.

9 (*a*) S. H. Hwang, J. H. Paek and S. S. Lim, *Molecules*, 2016, **21**, 1609; (*b*) H. Y. Muti and S. Olimat, *Orient. J. Chem.*, 2018, **34**, 2721.

10 G. Favaro, C. Clementi, A. Romani and V. Vickackaite, *J. Fluoresc.*, 2007, **17**, 707.

11 (*a*) H. Liu, X. Zhong, Q. Pan, Y. Zhang, W. Deng, G. Zou, H. Hou and X. Ji, *Coord. Chem. Rev.*, 2024, **498**, 215468; (*b*) F. Liu, X. Lai, S. Zhao, Z. Lu, P. Han and L. Chen, *Food Chem.*, 2023, **402**, 134251; (*c*) C. Liu, Y. Mei, Q. Lei, X. Ma, X. Nan, Y. Zhu, J. Liao, Y. Xu, Y. Luo, H. Zhang, M. Yang, X. Lin and Q. Huang, *Chem. Eng. J.*, 2024, **499**, 156434.

12 (*a*) E. K. Adotey, M. A. Torkmahalleh, L. Tastanova, A. Bekeshev, D. Shah, P. K. Hopke, W. Lee and M. P. Balanay, *J. Hazard. Mater.*, 2024, **462**, 132671; (*b*) X. Hu, J. Shi, Y. Shi, X. Zou, H. E. Tahir, M. Holmes, W. Zhang, X. Huang, Z. Li and Y. Xu, *Meat Sci.*, 2019, **147**, 127; (*c*) H. M. Junaid, A. R. Solangi and M. Batool, *Analyst*, 2021, **146**, 2463.

13 For selected examples see: (*a*) R. Zhang, Y. Zheng, Q. Zhang, Z. Wu, L. Wang, J. Zhang, H. Ren and E. Duan, *J. Environ. Chem. Eng.*, 2024, **12**, 112391; (*b*) S. Liu, Z. Wu, N. Nian, P. Zhang and L. Ni, *Water, Air, Soil Pollut.*, 2024, **235**, 449; (*c*) S. Liu, Y. Zhang, Y. Zhang, J. Zhang, R. Tian and L. Zhao, *Diamond Relat. Mater.*, 2024, **148**, 111382; (*d*) M. He, X. Fu, G. Du, H. Li, P. Zhao and X. Liu, *Packag. Technol. Sci.*, 2023, **36**, 465; (*e*) X. Mei, D. Wang, S. Wang, J. Li and C. Dong, *Anal. Bioanal. Chem.*, 2022, **414**, 7253; (*f*) A. Tall, F. A. Cunha, B. Kaboré, C. A. E. S. Barbosa, U. Rocha, T. O. Sales, M. O. F. Goulart, I. Tapsoba and J. C. C. Santos, *Microchem. J.*, 2021, **166**, 106219; (*g*) H. Tian, G. Ju, M. Li, W. Fu, Y. Dai, Z. Liang, Y. Qiu, Z. Qin and X. Yin, *RSC Adv.*, 2021, **11**, 35946; (*h*) Z. Ma, Y. Ma, M. Gu, X. Huo, S. Ma, Y. Lu, Y. Ning, X. Zhang, B. Tian and Z. Feng, *Nanomaterials*, 2020, **10**, 1924.

14 (*a*) Y. Wang, X. Hou, Y. Li, X. Sun, R. Hu, Y. Lv, R. Jia and L. Ding, *Microchem. J.*, 2024, **206**, 111562; (*b*) S. Zhang, Z. Wang, W. Yan and Y. Gou, *Spectrochim. Acta, Part A*, 2021, **259**, 119887; (*c*) Q. Sun, Y. Long, S. Pan, H. Liu, J. Yang and X. Hu, *Luminescence*, 2018, **33**, 1401.

15 (*a*) S. Miao, K. Liang, J. Zhu, B. Yang, D. Zhao and B. Kong, *Nano Today*, 2020, **33**, 100879; (*b*) Q. Xu, T. Kuang, Y. Liu, L. Cai, X. Peng, T. S. Sreeprasad, P. Zhao, Z. Yu and N. Li, *J. Mater. Chem. B*, 2016, **4**, 7204.

16 (*a*) A. Saravanan, P. Das, M. Maruthapandi, S. Aryal, S. Michaeli, Y. Mastai, J. H. T. Luong and A. Gedanken, *Surf. Interfaces*, 2024, **46**, 103857; (*b*) P. Das, S. Ganguly, S. Mondal, M. Bose, A. K. Das, S. Banerjee and N. C. Das, *Sens. Actuators, B*, 2018, **266**, 583.

17 F. Wang, Y. Zhang, H. Li, W. Gong, J. Han, S. Jiang, D. Li and Z. Yao, *Food Chem.*, 2025, **463**, 141122.

18 P. Zhou, J. Xu, X. Hou, L. Dai, J. Zhang, X. Xiao and K. Huo, *Int. J. Biol. Macromol.*, 2023, **253**, 126714.

19 (*a*) Z. Zhu, X. Li, M. Luo, M. Chen, W. Chen, P. Yang and X. Zhou, *J. Colloid Interface Sci.*, 2022, **605**, 330; (*b*) S. K. Park, H. Lee, M. S. Choi, D. H. Suh, P. Nakhanivej and H. S. Park, *Energy Storage Mater.*, 2018, **12**, 331.

20 (*a*) W. Lu, Y. Guo, J. Zhang, Y. Yue, L. Fan, F. Li, C. Dong and S. Shuang, *ACS Appl. Mater. Interfaces*, 2022, **14**, 57206; (*b*) S. Huang, E. Yang, J. Yao, X. Chu, Y. Liu, Y. Zhang and Q. Xiao, *ACS Omega*, 2019, **4**, 9333; (*c*) H. Behboudi, M. Pourmadadi, M. Omidi, M. Rahmandoust, S. O. R. Siadat and J. S. Shayeh, *Surf. Interfaces*, 2022, **29**, 101710; (*d*) M. Yang, J. Yao, B. Su, N. Xin, T. Zhou, M. Zeng, C. Wu, D. Wei, J. Sun and H. Fan, *J. Mater. Chem. B*, 2023, **11**, 5898; (*e*) P. Fan, C. Liu, C. Hu, F. Li, X. Lin, S. Yang and F. Xiao, *New J. Chem.*, 2022, **46**, 2526; (*f*) X. Li, S. Ding, Z. Lyu, P. Tieu, M. Wang, Z. Feng, X. Pan, Y. Zhou, X. Niu, D. Du, W. Zhu and Y. Lin, *Small*, 2022, **18**, 2203001; (*g*) W. Kong, C. Li, Z. Sun, F. Gao, J. Zheng and Y. Jiang, *Molecules*, 2023, **28**, 5526.

21 (*a*) Q. Miao, Y. Li, X. Fan, D. Deng, X. Yan, H. He and L. Luo, *Analyst*, 2021, **146**, 6297; (*b*) S. K. Tammina, Y. Wan, Y. Li and Y. Yang, *J. Photochem. Photobiol., B*, 2020, **202**, 111734; (*c*) Q. Xu, W. Cai, M. Zhang, R. Su, Y. Ye, Y. Li, L. Zhang, Y. Guo, Z. Yu, S. Li, X. Lin, Y. Chen, Y. Luo, J. Street and M. Xu, *RSC Adv.*, 2018, **8**, 17254.

22 L. Amaral and A. Daniel-da-Silva, *Molecules*, 2022, **27**, 6782.

23 Z. Liang, R. Shen, Y. H. Ng, P. Zhang, Q. Xiang and X. Li, *J. Mater. Sci. Technol.*, 2020, **56**, 89.

24 X. Fu, J. Huang, X. Zhu, J. Rong, Z. Lin, Y. Dong and F. Fu, *Chem. Commun.*, 2022, **58**, 7180.

25 (*a*) P. Li, F. Han, W. Cao, G. Zhang, J. Li, J. Zhou, X. Gong, G. Turnbull, W. Shu, L. Xia, B. Fang, X. Xing and B. Li, *Appl. Mater. Today*, 2020, **19**, 100601; (*b*) F. Nemati, R. Z. Dorabei, M. Hosseini and M. R. Ganjali, *Sens. Actuators, B*, 2018, **255**, 2078.

26 S. Kadian and G. Manik, *Food Chem.*, 2020, **317**, 126457.

27 (*a*) B. Thangaraj, P. R. Solomon, S. Chuangchote, N. Wongyao and W. Surareungchai, *ChemBioEng Rev.*, 2021, **8**, 265; (*b*) J. Singh, S. Kaur, J. Lee, A. Mehta, S. Kumar, K. H. Kim, S. Basu and M. Rawat, *Sci. Total Environ.*, 2020, **720**, 137604; (*c*) S. Elkun, M. Ghali, T. Sharshar and M. M. Mosaad, *Sci. Rep.*, 2024, **14**, 27927.

28 W. Gao, H. Song, X. Wang, X. Liu, X. Pang, Y. Zhou, B. Gao and X. Peng, *ACS Appl. Mater. Interfaces*, 2017, **10**, 1147.

29 W. Lu, Y. Jiao, Y. Gao, J. Qiao, M. Mozneb, S. Shuang, C. Dong and C. Li, *ACS Appl. Mater. Interfaces*, 2018, **10**, 42915.

30 C. Pan, T. Chen, L. Ma, X. Qin, Q. Wen and S. Feng, *Chin. J. Anal. Chem.*, 2022, **50**, 100069.

31 L. Dong, J. Wang, Y. Ma, Y. Ruan, Z. Hu and X. Ma, *Arab. J. Chem.*, 2024, **17**, 105660.

32 X. Lin, J. Chen, L. Zhang, T. Lan, Y. Yu, Z. Ke, L. Hu and Z. Zhang, *Chin. J. Struct. Chem.*, 2010, **29**, 437.

33 W. Kong, C. Li, Z. Sun, F. Gao, J. Zheng and Y. Jiang, *Molecules*, 2023, **28**, 5526.

34 J. Li, L. Zhang, P. Li, Y. Zhang and C. Dong, *Sens. Actuators, B*, 2018, **258**, 580.

35 (*a*) S. Huang, E. Yang, J. Yao, X. Chu, Y. Liu, Y. Zhang and Q. Xiao, *ACS Omega*, 2019, **4**, 9333; (*b*) Q. Yang, W. Yang, Y. Zhang, W. Ge, X. Yang and P. Yang, *Nanomaterials*, 2020, **10**, 460.

36 J. Wang, H. Wei, X. Chen, C. Chen and X. Chen, *Int. J. Hydrogen Energy*, 2020, **45**, 595.
37 L. Zhu, D. Shen and K. Luo, *J. Colloid Interface Sci.*, 2022, **617**, 557.
38 Y. Yan, L. Li, H. Zhang, F. Du, Y. Meng, S. Shuang, R. Wang, S. Song and C. Dong, *Spectrochim. Acta, Part A*, 2021, **256**, 119751.
39 Y. Mao, S. Gao, L. Yao, L. Wang, H. Qu, Y. Wu, Y. Chen and L. Zheng, *J. Hazard. Mater.*, 2021, **408**, 124898.
40 C. Ni, W. Zhang, W. Bi, M. Wu, S. Feng, X. Chen and L. Qu, *RSC Adv.*, 2024, **14**, 26667.
41 X. Sun, M. Yuan, B. Liu and J. Shen, *RSC Adv.*, 2018, **8**, 19786.
42 J. Xu, Y. Gao, L. Qin, X. Yue, Q. Zhang and L. Wang, *Ceram. Int.*, 2023, **49**, 7546.
43 W. He, Z. Huo, X. Sun and J. Shen, *Microchem. J.*, 2020, **153**, 104528.
44 M. Lu, C. Pan, X. Qin and M. Wu, *ACS Omega*, 2023, **8**, 14499.
45 Y. Luo, C. Cui, X. Zhang, Y. Jiang, Z. Xiang, C. Ji and Z. Peng, *Molecules*, 2023, **28**, 1566.
46 W. Chen, H. Lin, Y. Wu, M. Yang, X. Zhang, S. Zhu, M. He, J. Xie and Z. Shi, *Adv. Compos. Hybrid Mater.*, 2022, **5**, 2378.
47 H. Wu, L. Pang, M. Fu, X. Guo and H. Wang, *J. Pharmaceut. Biomed. Anal.*, 2020, **180**, 113052.